



ISOSTATICALLY DISTURBED TERRAIN OF NORTHWESTERN ANDES MOUNTAINS FROM SPECTRALLY CORRELATED FREE-AIR AND GRAVITY TERRAIN DATA

Orlando Hernández P.^{1,2} and Ralph R. B. von Frese ¹

(1) Dept. of Geological Sciences, The Ohio State University, Columbus, OH 43210 USA, FAX 614 2927688. hernandez.135@osu.edu , vonfrese@geology.ohio-state.edu,

(2) Dept. of Geosciences, Universidad Nacional de Colombia, Bogotá, D.C. COLOMBIA ohernandezp@unal.edu.co

ABSTRACT

Recently revised models on global tectonics describe the convergence of the North Andes, Nazca, Caribbean and South American Plates and their seismicity, volcanism, active faulting and extreme topography. The current plate boundaries of the area are mainly interpreted from volcanic and seismic datasets with variable confidence levels. New insights on the isostatic state and plate boundaries of the northwestern Andes Mountains can be obtained from the spectral analysis of recently available gravity and topography data.

Isostatically disturbed terrain produces free-air anomalies that are highly correlated with the gravity effects of the terrain. The terrain gravity effects (TGE) and free air gravity anomalies (FAGA) of the Andes mountains spectral correlation data confirms that these mountains are isostatically disturbed. Strong negative terrain-correlated FAGA along western South America and the Greater and Lesser Antilles are consistent with anomalously deepened mantle displaced by subducting oceanic plates. Inversion of the compensated terrain gravity effects (CTGE) reveals plate subduction systems with alternating shallower and steeper subduction angles. The gravity modeling highlights crustal deformation from plate collision and subduction and other constraints on the tectonism of the plate boundary zones for the region.

Keywords: North Andes, Isostasy, Gravity, Moho.

RESUMEN

Modelos recientes de tectónica de placas describen la convergencia de las placas de los Andes del Norte, Nazca, Caribe y Sur América y su sismicidad, volcanismo, fallamiento activo y topografía extrema. Los actuales límites tectónicos del área han sido interpretados a partir de bases de datos con varios niveles de confiabilidad. Nueva información sobre el estado isostático y bordes tectónicos de los Andes del noroeste de Sur América puede ser obtenida del análisis espectral de datos de topografía y gravimetría disponibles recientemente. Terrenos isostáticamente distorsionados producen anomalías de aire libre que son altamente correlacionadas con los efectos gravimétricos

Manuscript received April 19 2006.

Accepted for publication October 29 2006.

del terreno. Los efectos topográficos del terreno espectralmente correlacionables con las anomalías gravimétricas de aire libre de las montañas de los Andes confirman que estas montañas están distorsionadas isostáticamente. Fuertes anomalías negativas de aire libre correlacionables con los efectos gravimétricos del terreno a lo largo del margen oeste de Sur América y las Antillas Mayores y Menores son consistentes con un manto anómalamente mas profundo desplazado por la subducción de placas de corteza oceánica. El modelamiento inverso de las anomalías gravimétricas revela sistemas de subducción con inclinaciones sub-horizontales y verticales alternantes. El modelamiento gravimétrico resalta la deformación cortical producto de la colisión de placas y subducción y otras características del tectonismo de zonas de límites de placas de la región.

Palabras claves: Andes del Norte, Isostasia, Gravimetría, MOHO.

1. INTRODUCTION

(Leftwich *et al.*, 2005).

The tectonic setting of northwestern South America is poorly understood because of the complex interaction of numerous tectonic plates, and the scarce and incomplete geologic mapping due to the dense vegetation cover and limited accessibility to remote areas. International scientific interest in the northwestern Andes Mountains is intense because it is the key to improve our understanding of the geological evolution of the backbone of America and the Caribbean, and related volcanic and seismic hazards (Bird, 2003; Cediel *et al.*, 2003). The ability of current physical models to predict neotectonic and other intra-plate lithospheric stresses and strain is limited because the structures and geometry of plate boundaries are largely hidden and poorly understood. However, the deployment of geodetic sensors including the GPS-derived ground velocities and high resolution topography have substantially improved the modeling of the lithosphere to analyze surface mass dynamics (Kellogg *et al.*, 1985; Kellogg *et al.*, 1995).

In this paper, spectral correlation theory (e.g., Leftwich *et al.*, 2005; von Frese and Tan, 1999) is applied to terrain and free-air gravity anomalies for new constraints on the boundary zones of the North Andes and Panama Microplates, and the Cocos, Nazca, Caribbean and South American Plates. Normalization and local favorability indexes are implemented to facilitate the visualization and interpretation of gravity anomalies. This methodology has been applied and validated in other crustal studies such as East Asia (Tan and von Frese, 1997), Antarctica (von Frese *et al.*, 1992; 1999), Greenland (Roman, 1999), Ohio (Kim *et al.*, 2000), and Iceland

Isostatically disturbed terrain produces free-air anomalies that are highly correlated with the gravity effects of the terrain. Spectral correlation of the terrain gravity effects (TGE) and free-air gravity anomalies (FAGA) suggested that the Andes Mountains are isostatically disturbed with an anomalous underlying crust-mantle interface (MOHO). Strong negative terrain-correlated FAGA along western South America and the Greater and Lesser Antilles are consistent with anomalously deepened mantle displaced by subducting oceanic plates. Gravity estimates regionally augment and extend the seismic estimates to highlight crustal deformation from plate collision and subduction in northwestern South America. The gravity anomalies are consistent with a complex evolution for northwestern South America involving the accretion of an oceanic plateau with strong Caribbean affinities, obduction of the oceanic crust, over thrusting and strike-slip faulting. These tectonic characteristics are not readily accounted for by the conventional model of “Andean Type” orogenesis of the Central Andes (Liu *et al.*, 2002).

2. SPECTRALLY CORRELATED FREE-AIR AND TERRAIN GRAVITY

The isostasy of northwestern South America was investigated considering the topography and bathymetry data from National Imagery and Mapping Agency (NIMA) from -8°S to 23.5°N latitude and from -90°W to -58.5°W longitude. Surface and bathymetry elevations from the JGP95E terrain data base (Smith and Sandwell, 1994, 1997) were processed to produce the

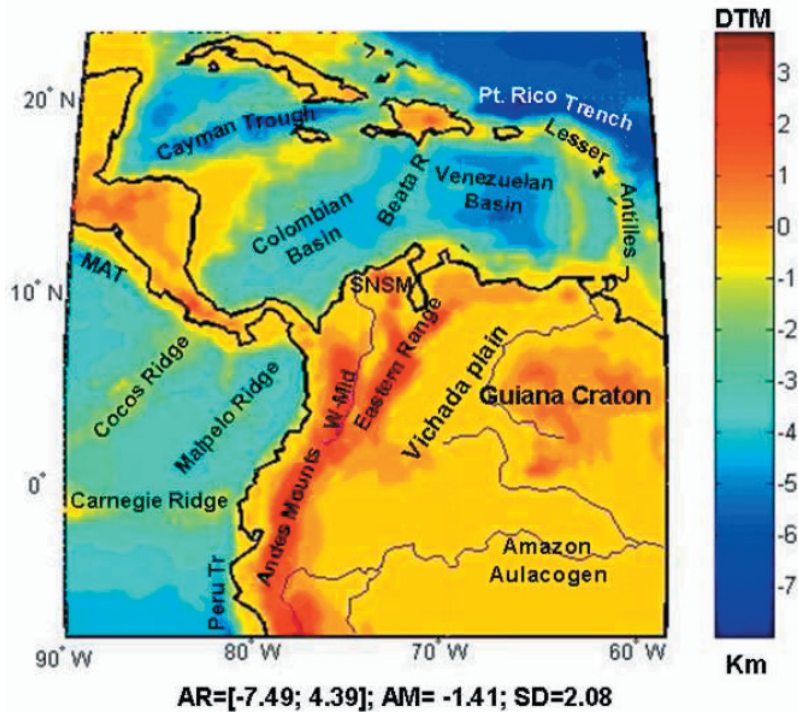


Figure. 1. Topography/bathymetry of northwestern South America with superposed regional tectonic features between -8°S to 23.5°N latitude and from -90°W to -58.5°W longitude. Map annotations include the amplitude range (AR) of (min; max) values, the amplitude mean (AM) and standard deviation (SD). SNSM= Sierra Nevada of Santa Martha, W-Mid = Western-Central ranges. This map was produced using the Albers equal-area conic projection.

Digital Elevation Model (DEM) in Figure 1 for the water and rock terrain gravity components at 0.5° nodal spacing. Free-air gravity anomalies (FAGA) were estimated from the EGM96 spherical harmonic Earth Gravity Model to degree and order 360 (Lemoine *et al.*, 1998) at 20 km altitude over the $32^{\circ} \times 32^{\circ}$ area at 0.5° nodal spacing in Figure 2. The altitude of 20 km was chosen to help minimizing the effects of local density errors in the terrain gravity modeling (e.g., Leftwich *et al.*, 2005).

The terrain gravity effects were modeled in spherical coordinates at 20 km altitude by Gauss-Legendre Quadrature integration in Figure 3 (von Frese, 1980). The terrain gravity modeling used densities of 2.8 gm/cm^3 for the crust and 1.03 gm/cm^3 for oceanic water. Spectral correlation theory was used to analyze the co-registered FAGA and TGE for their anomaly correlations using MatLab (MATHWORKS, 2005). Specifically, the Fourier transforms T and F of TGE and FAGA, respectively, were used to

obtain their correlation spectrum (Davis, 1986; von Frese *et al.*, 1997a, Kim *et al.*, 2000) given by:

$$CC(k) = \cos(\Delta\theta k) = \text{Re} \left[\frac{F(k) |T(k)|}{T(k) |F(k)|} \right] \quad (1)$$

Where $CC(k)$ is the correlation coefficient between the k^{th} wave numbers components $F(k)$ and $T(k)$, and denotes taking the real parts of the wave number components. Usually, $CC(k)$ is evaluated from the cosine of the phase difference ($\Delta\theta k$) between the two k^{th} wave number components.

Using the correlation spectrum between FAGA and TGE, spectral correlation filters were designed to extract terrain-correlated

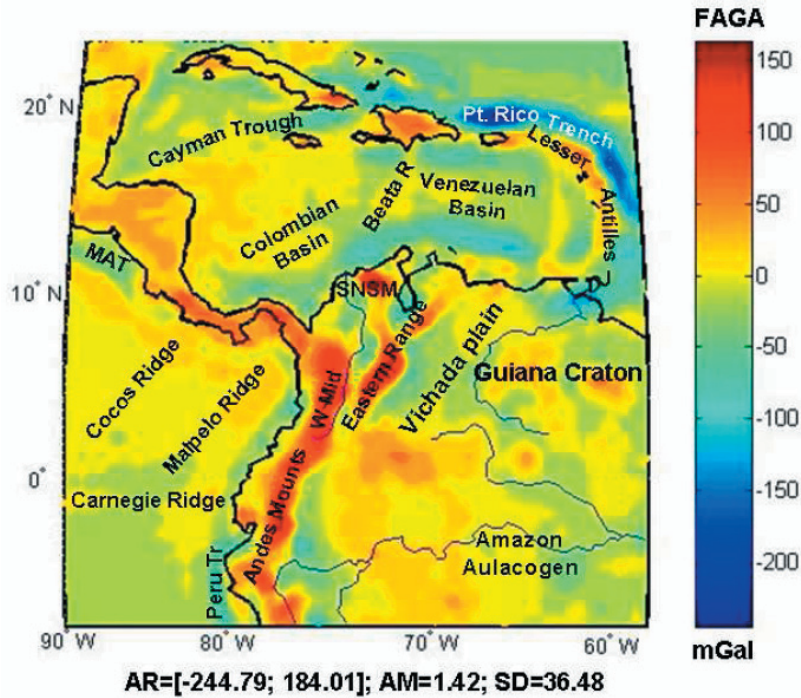


Figure. 2. Free-air gravity anomalies (FAGA) at 20 km elevation for the study region (Lemoine, et al., 1998). Map annotations include the amplitude range (AR) of (min; max) values, the amplitude mean (AM) and standard deviation (SD). SNSM= Sierra Nevada of Santa Martha, W-Mid = Western-Central ranges. This map was produced using the Albers equal-area conic projection..

free-air gravity signals. Those wave numbers components showing intermediate to high positive ($CC_p(k) \geq 0.3$) and negative ($CC_n(k) \leq 0.3$) correlations were identified. The cut off values for the correlation filter were determined to minimize correlative features between the terrain-decorrelated free-air and compensating terrain gravity components. In the other hand, transforming positively and negatively correlated free-air wave number components according to the selected cut off values yielded the terrain-correlated free air gravity anomalies (TCFAGA) in Figure 4. The residual terrain-decorrelated free-air gravity anomalies (TDFAGA) in Figure 5 were calculated by subtracting TCFAGA from FAGA, so that

$$\text{FAGA} = \text{TCFAGA} + \text{TDFAGA} \quad (2)$$

TCFAGA are explained by anomalies associated with the topography while TDFAGA include the gravity effects of sources within the crust (e.g., local bodies) and the sub-crust.

Similarly, spectral correlation filters were used to extract FAGA-correlated TGE (FCTGE) in Figure 6 and FAGA-decorrelated TGE (FDTGE) in Figure 7. The FCTGE sharpen up the TGE components that may be isostatically disturbed, whereas the FDTGE involves relatively marginal amplitudes that appear to reflect mostly noise in the data and other non-geological effects.

3. ANALYSIS OF ANOMALY CORRELATIONS

TCFAGA and FCTGE were normalized to facilitate recognizing the anomaly correlations between them (von Frese *et al.*, 1997). To enhance the visual perception of the anomaly correlations, the following transformation was applied:

$$Z_i(X) = \sigma_Z \left(\frac{x_i - \mu_X}{\sigma_X} \right) + \mu_Z \quad (3)$$

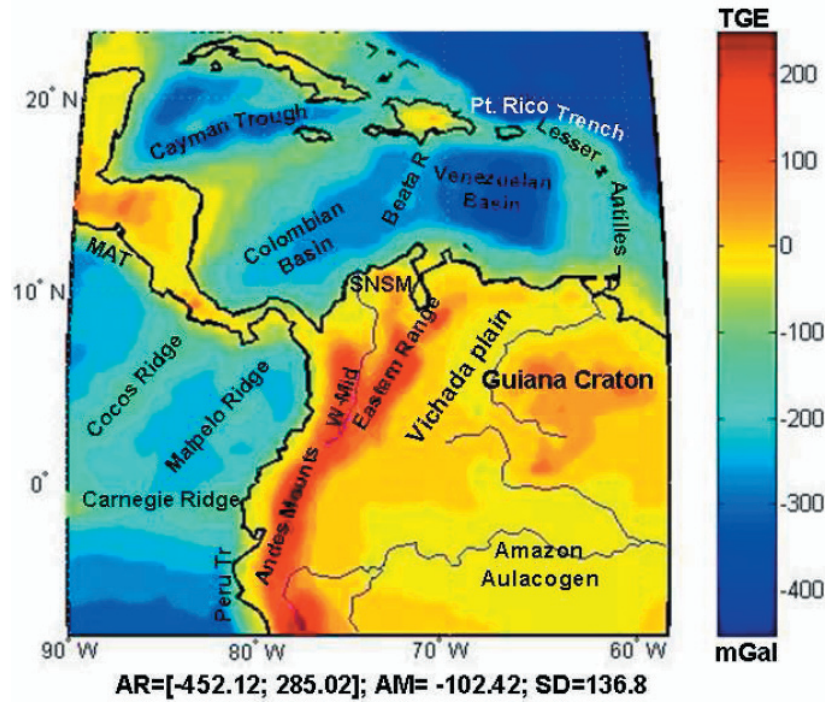


Figure 3. Terrain Gravity Effects (TGE) at 20 km elevation for the study region by Gauss-Legendre quadrature integration. Map annotations include the amplitude range (AR) of (min; max) values, the amplitude mean (AM) and standard deviation (SD). SNSM= Sierra Nevada of Santa Martha, W-Mid = Western-Central ranges. This map was produced using the Albers equal-area conic projection.

Where μ_x and σ_x both represent the respective values of the mean and standard deviation of the signal X. The expression in parentheses standardizes the xi coefficients to zero mean and unit standard deviation and is dimensionless. However, the values for mean μ_Z and standard deviation of μ_Z of the normalized signal Z can be specified by the user to facilitate the visual analysis.

The transformations of TCFAGA and FCTGE used the normalization of $Z = 10$ to facilitate plotting the two datasets with common plotting parameters (von Frese *et al.*, 1997). Local favorability indices (Merriam and Sneath, 1966) were used to highlight the various anomaly correlations in the normalized TCFAGA and FCTGE. Positively correlated features were mapped out by summed local favorability indexes (SLFI) obtained by (4):

$$SLFI_i = \frac{(z_i(X)) - \mu_Z}{\sigma_Z} + \frac{(z_i(Y) - \mu_Z)}{\sigma_Z} \quad (4)$$

In equation (4), Z(X) and Z(Y) were both respectively the normalized TCFAGA and FCTGE coefficients. The peak-to-peak correlations between the two data sets were mapped out by $SLFI_i \geq 8.7226$ in Figure 8, whereas trough-to-trough correlations were mapped out by the coefficients satisfying $SLFI_i \leq -8.7226$ in Figure 9. The SLFI coefficients brought out the positively or directly correlated features, while suppressing the negatively and null correlated features between TCFAGA and FCTGE.

To enhance the perception of inversely correlated features obtained from wave numbers with negative correlation coefficients, the normalized and scaled datasets were subtracted cell by cell for differenced local favorability indexes (DLFI) by (5):

$$DLFI_i = \frac{(z_i(X)) - \mu_Z}{\sigma_Z} - \frac{(z_i(Y) - \mu_Z)}{\sigma_Z} \quad (5)$$

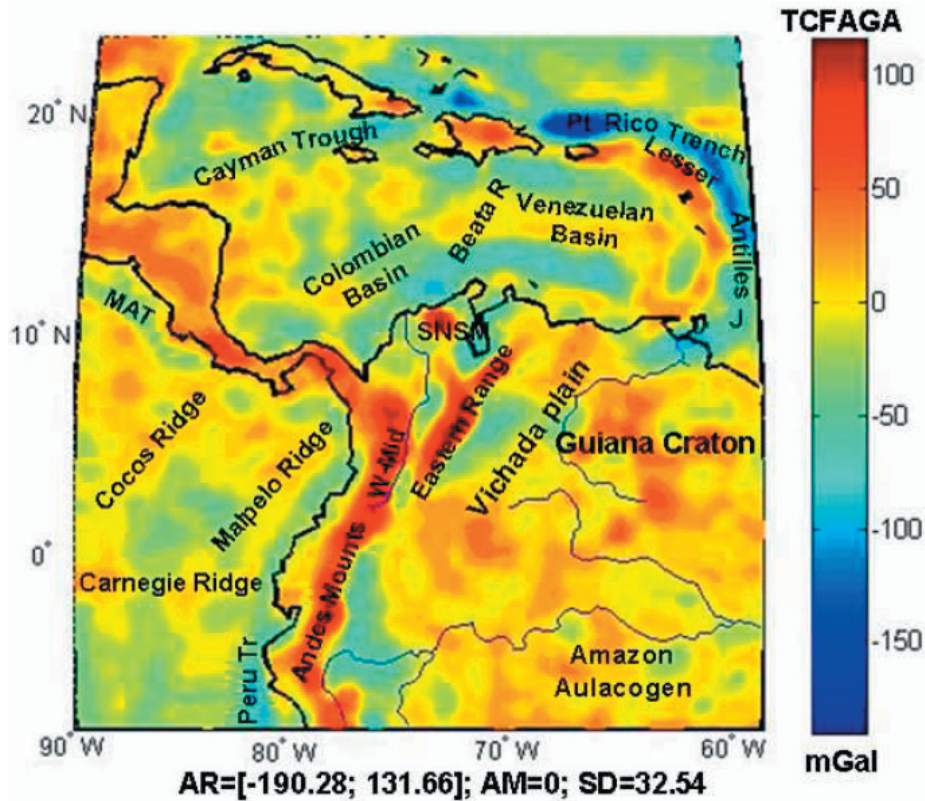


Figure. 4. Terrain-correlated FAGA (TCFAGA) at 20 km elevation for the study area. Map annotations include the amplitude range (AR) of (min; max) values, the amplitude mean (AM) and standard deviation (SD). SNSM = Sierra Nevada of Santa Martha, WMid = Western-Central ranges. This map was produced using the Albers equal-area conic projection.

CC	TGE	FCTGE	FDTGE	FAGA	TCFAGA	TDFAGA
TGE	1	0,97	0,24	0,52	0,59	0
FCTGE	0,97	1	0	0,56	0,6	0,05
FDTGE	0,24	0	1	-0,09	0	-0,02
FAGA	0,52	0,56	-0,09	1	0,89	0,45
TCFAGA	0,59	0,6	0	0,89	1	0
TDFAGA	0	0,05	-0,02	0,45	0	1

Table. 1. Correlation coefficients (CC) between the gravity anomalies at 20 km altitude for the area from -80°S to 23.5°N latitude and from -90°W to -58.5°W longitude in northwestern South America.

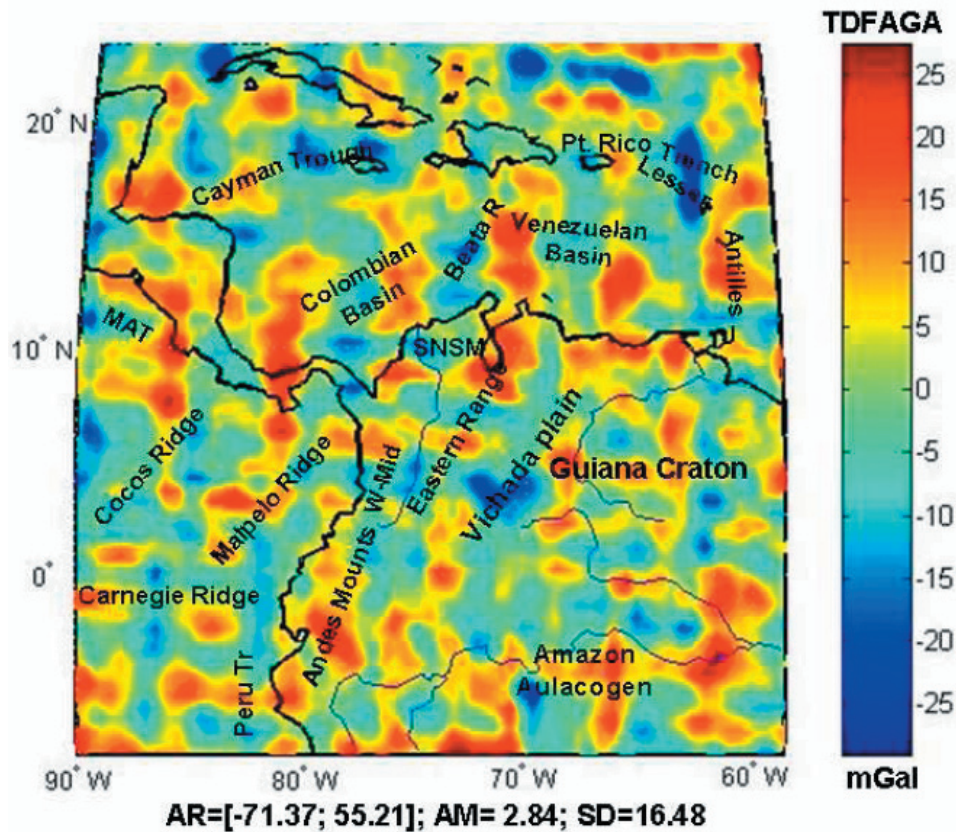


Figure 5. Terrain-decorrelated FAGA (TDFAGA) at 20 km elevation for the study area. Map annotations include the amplitude range (AR) of (min; max) values, the amplitude mean (AM) and standard deviation (SD). SNSM = Sierra Nevada of Santa Martha, W-Mid = Western-Central ranges. This map was produced using the Albers equal-area conic projection.

Positive features in TCFAGA which were correlative with negative FCTGE features (peak-to-trough) were mapped out by $DLFi \geq 4.8904$ in Figure 10, whereas negative TCFAGA that were correlative with positive FCTGE were mapped out by $DLFi \leq 4.8904$ in Figure 11. The DLFi coefficients emphasized the inversely correlated features, while suppressing the positively and null correlated features between TCFAGA and FCTGE. Table 1 summarizes the correlations between FAGA and TGE and their correlated filtered components.

The increase in the CC between TCFAGA and TGE ($CC=0.59$) relative to the CC between the raw FAGA and TGE ($CC=0.52$) facilitates the isostatic analysis of the tectonic features of the study area. However, the increase in the CC between TCFAGA and FCTGE ($CC=0.6$) with respect to the CC between TCFAGA and TGE ($cc=0.59$) is negligible and the physical meaning of FCTGE and FDTGE is obscured.

The CC between TDFAGA and FAGA ($CC=0.45$) is significant in showing the strong influence of the data-grid in the anomaly decomposition of FAGA in TCFAGA and TDFAGA. Therefore, further analyses of TDFAGA are required.

4. RESULTS

Isostatically disturbed terrains have gravity effects that directly correlate with FAGA. The complementary TDFAGA reflect the effects of lateral density variations in the crust, mantle and core, as well as errors in the data and data processing. In the subsections below, the gravity effects of the DTM and spectral correlations with free-air gravity anomalies are interpreted for constraints on the tectonic features of the study region.

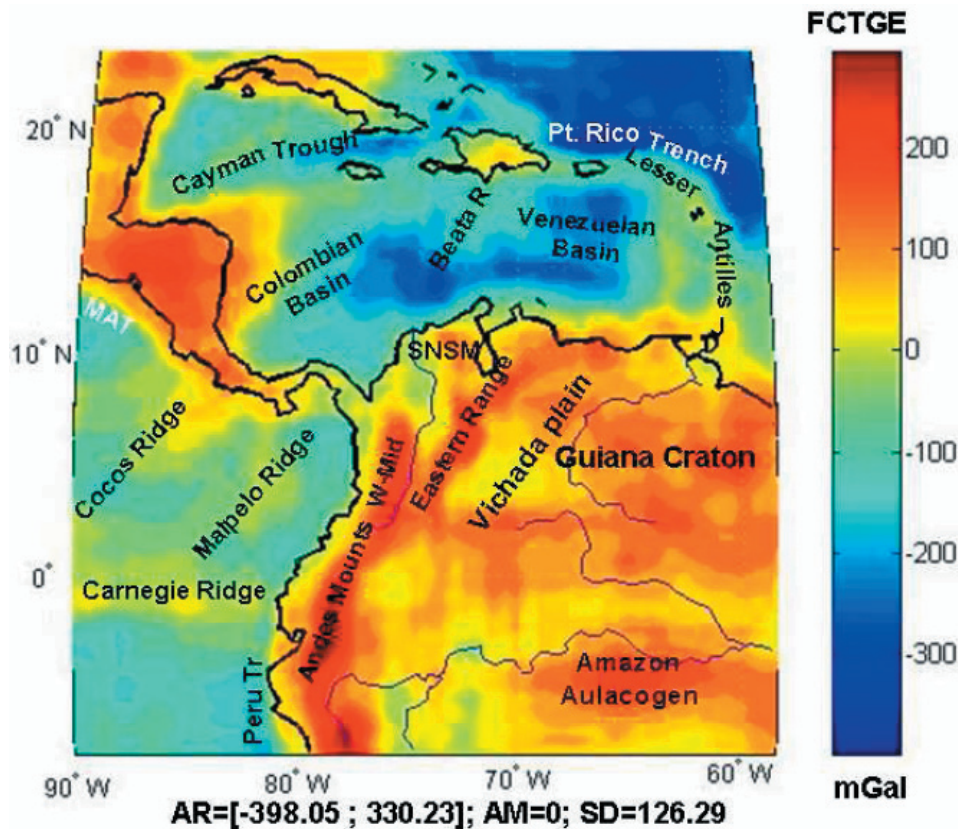


Figure 6. FAGA-correlated TGE (FCTGE) at 20 km elevation for the study area. Map annotations include the amplitude range (AR) of (min; max) values, the amplitude mean (AM) and standard deviation (SD). SNSM = Sierra Nevada of Santa Martha, W-Mid = Western-Central ranges. This map was produced using the Albers equal-area conic projection.

4.1. DIGITAL TERRAIN MODEL (DTM)

The DTM in Figure 1 presents major morphological and tectonic features that produce strong terrain gravity effects in the gravity anomalies. The topography data are increasingly being integrated into the techniques to study plate boundary zones (Stein & Freymueller, 2002). One approach is to use digital terrain models (DTM) showing the forms of mountain ranges, oceanic trenches, volcanic ridges and island arcs, and oceanic basins to constrain models of the processes that produced them. The DTM of northwestern South America suggests a complex tectonic setting with mountain building and uplift as a consequence of the plate convergences that have created the North Andes Mountains, the Sierra Nevada of Santa Marta and the Cordillera Central Mountains. Flat low lands are associated with the stable cratonic terrains of the Guiana Shield. Deep Pacific Ocean trenches along the

Peru - Ecuador - Colombia coastline and the Middle America Trench are associated with subduction zones. The Puerto Rico Trench in the Caribbean is associated with the Caribbean – North American subduction zone. The submarine Carnegie, Cocos and Malpelo volcanic ridges are associated with the Galapagos hot spot. The volcanic arc islands of the Lesser and Greater Antilles reflect intensive geodynamics in the region, including high seismicity and volcanic activity.

4.2. FREE-AIR GRAVITY ANOMALIES (FAGA)

The free air gravity anomalies in Figure 2 include the superposed gravity effects of the terrain and subsurface gravity variations. The FAGA amplitudes are smaller than the TGE amplitudes reflecting partial isostatic compensation of the terrain. However, the mean FAGA of 17 mGals

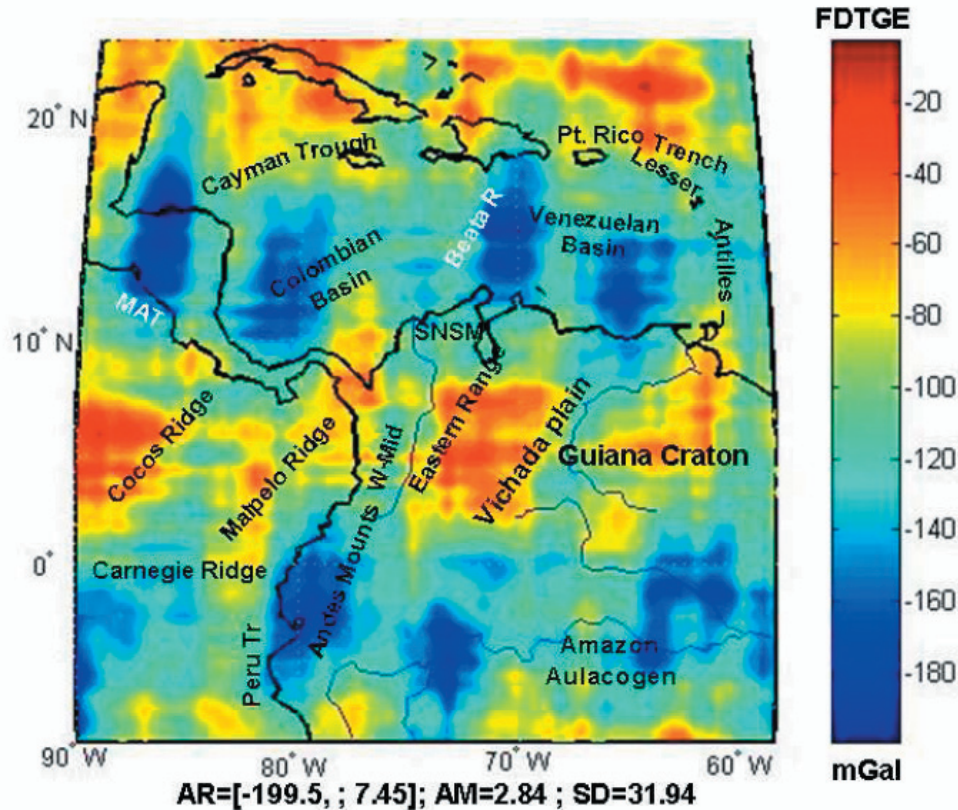


Figure 7. FAGA-decorrelated TGE (FDTGE) at 20 km elevation for the study area. Map annotations include the amplitude range (AR) of (min; max) values, the amplitude mean (AM) and standard deviation (SD). SNSM = Sierra Nevada of Santa Martha, WMid = Western-Central ranges. This map was produced using the Albers equal-area conic projection.

indicates that the mean terrain is isostatically disturbed. The largest negative anomalies are over the subduction zones, whereas the strongest positive FAGA are over the Andes Mountains and Sierra Nevada of Santa Marta. Moderate positive and negative FAGA are distributed along the oceanic volcanic ridges, Guiana Craton and oceanic plates. The positive correlation between TGE and FAGA ($CC = 0.52$) reflects the predominant condition of isostatically disturbed terrain in the tectonically complex study region.

4.3. TERRAIN GRAVITY EFFECTS

The terrain gravity effects (TGE) in Figure 3 produced by crust - air (2.8 gm/cm^3) and crust - water (1.82 gm/cm^3) interfaces are the highest density contrasts that can be defined by the lithosphere. Therefore, the minimum and maximum TGE values of -452.12 mGals and 285.02 mGals , respectively, are also the

extreme values that FAGA could take in a case of 0% isostatic compensation. Negative TGE ($TGEmean = -51.21 \text{ mGals}$) are stronger over the Caribbean Sea than the Pacific Ocean. Negative TGE overlie the Puerto Rico Trench, Cayman Trough, and Colombian and Venezuelan Basins. The Beata Ridge, Lesser and Greater Antilles have relatively positive TGE. In the Pacific, negative TGE overlie the Panama Basin and the Peru Trench, and positive TGE overlie the Carnegie, Cocos and Malpelo Ridges. At the continent, positive TGE reflect the presence of the mountainous Central America, Andes Mountains, Sierra Nevada of Santa Martha and the Guiana Craton. Relatively negative anomalies are associated with the Vichada Plain and Amazon River Aulacogens.

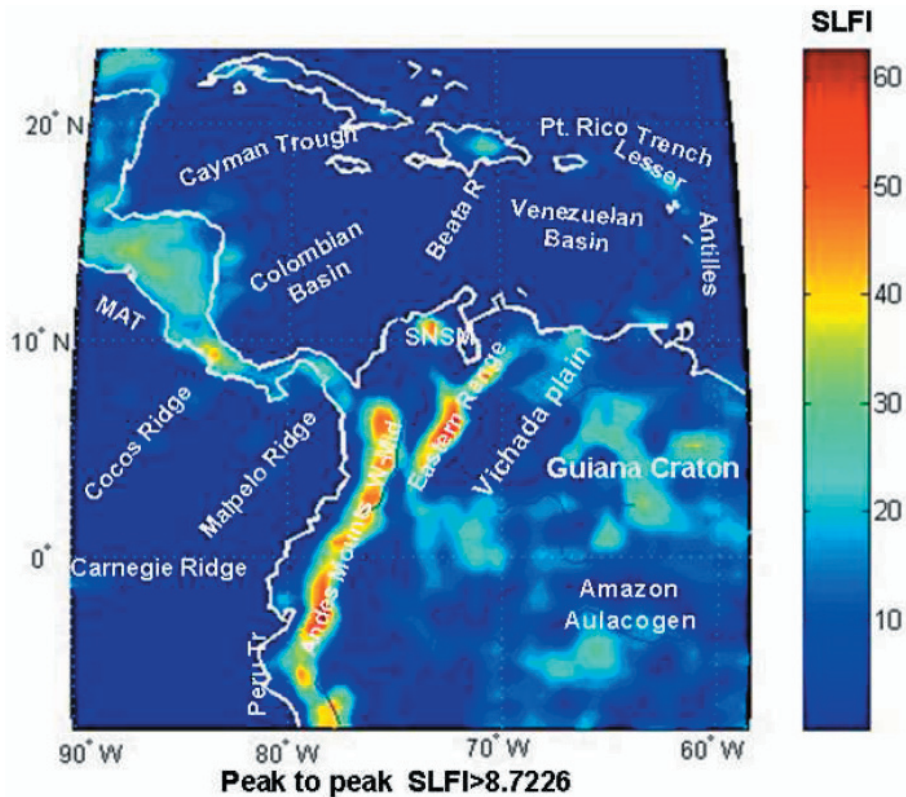


Figure 8. Summed local favorability indices (SLFI) for TCFAGA and FCTGE at 20 km elevation for the study region showing TCFAGA-peak to FCTGE-peak correlations for SLFI , 8.7226. SNSM= Sierra Nevada of Santa Martha, W-Mid = Western-Central ranges. This map was produced using the Albers equal-area conic projection.

4.4. TERRAIN-CORRELATED FREE-AIR GRAVITY ANOMALIES

TCFAGA in Figure 4 have a more complex anomaly pattern than TGE inferring a wide range of isostatic disturbances of the terrain. TCFAGA varies from -190.28 to 131.66 mGals, with a mean value of zero. Thus, the TCFAGA reflect both negative and positive disturbances of continental and oceanic features. Volcanic activity and mountain building are associated with positive TCFAGA, whereas negative TCFAGA characterize trenches and troughs. Arcuate positive and negative TCFAGA can be observed along the Greater and Lesser Antilles, along the Caribbean - North Andes subduction zone (Bird, 2003, CASA, 1998). Therefore, the subduction of the North American plate under the Caribbean Plate is well mapped from the TCFAGA. Negative TCFAGA beneath the trenches are due to the negative density contrast (- 0.37 gm/cm³) of the subducting oceanic slab into the mantle. Positive TCFAGA

over the recently formed volcanic islands are explained by oceanic crustal thickening which is not fully compensated. The TCFAGA are smaller than TGE, suggesting partial isostatic compensation from the thickening of the oceanic crust into the mantle. Negative TCFAGA are located along the Colombian - Venezuelan Basins and the Caribbean - North Andes subduction zone (Bird, 2003, CASA, 1998). The low TCFAGA amplitudes suggest that the Caribbean - North Andes subduction zone is incipient with respect to the Caribbean - North American or Nazca - North Andes subduction zones. In Central America, the positive TCFAGA from Panama to Costa Rica (60-80 mGals) and from Nicaragua to Honduras (20-40 mGals) are less prominent than the TCFAGA in the Andes (80-100 mGals) suggesting that Central America may be relatively more isostatically compensated than the Andes Mountains. The converging plate boundary between the Panama and North Andes Micro-plates proposed by Kellogg (1985) is

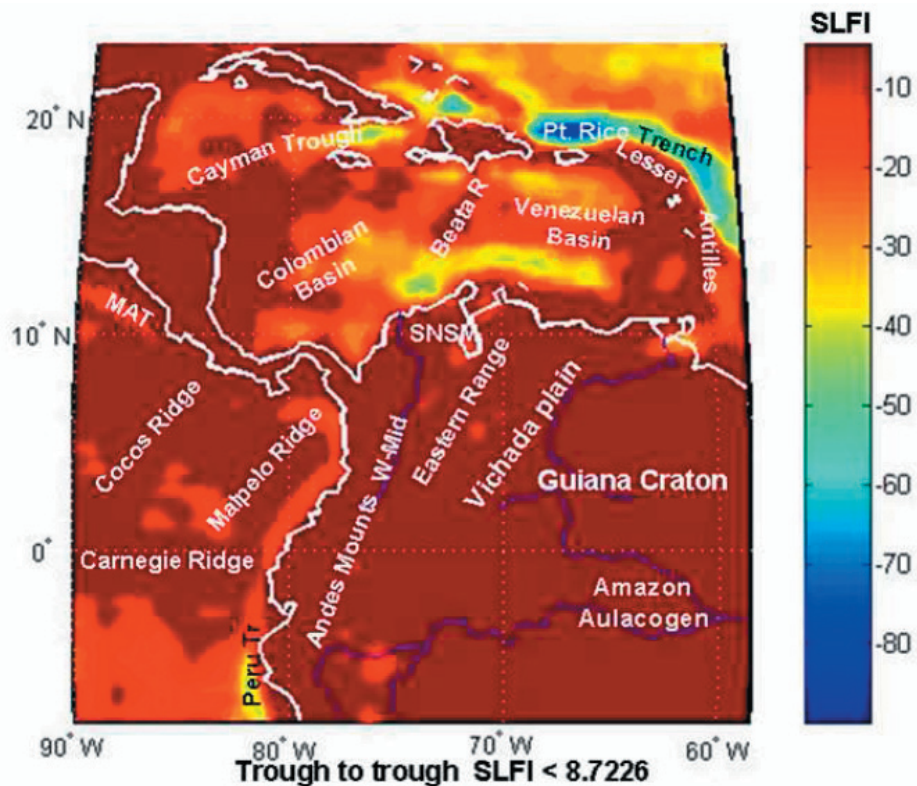


Figure. 9. Summed local favorability indices (SLFI) for TCFAGA and FCTGE at 20 km elevation for the study region showing the TCFAGA-trough to FCTGE-trough correlations for $SLFI \cdot -8.7226$. SNSM= Sierra Nevada of Santa Martha, W-Mid = Western-Central ranges. This map was produced using the Albers equal-area conic projection.

not supported by the TCFAGA which shows no distinct anomaly between them.

At the Pacific Ocean, negative TCFAGA clearly define the Middle America Trench. Relatively positive TCFAGA are associated with the flat slab subduction of the Cocos ridge under the Panama – Costa Rica Micro-plate. Negative TCFAGA along the western margin of South America vary from -10 to -60 mGals, being comparatively smaller in the Colombian Trench. These results reflect the lower angle of subduction of the Nazca plate in contrast to the steeper angles of subduction and negative amplitudes at the Chilean - Peruvian subduction zone. Relative TCFAGA highs are associated with the flat slab subduction of the Carnegie Ridge under the North Andes Micro-plate.

At the continent, positive TCFAGA at the Andes Mountains (90 to 130 mGals) show that these mountains are isostatically disturbed. A remarkable isolated positive TCFAGA anomaly

is located in northern Colombia, in the Sierra Nevada of Santa Marta (130 mGals). Here, the highest elevations of northwestern South America have also the maximum TCFAGA, showing that these mountains, reaching elevations of 5800 m, are even less compensated than the Andes Mountains suggesting that the Sierra Nevada of Santa Marta has been intensively deformed and uplifted after the Andean orogenesis.

It is not clear how these mountains were formed and why they occupy their present position. These mountains are perhaps allochthonous tectonic blocks that were moved from the east along a left lateral fault (Dewey and Pindell, 1985). The TCFAGA also support this explanation, which implies that lateral stress caused crustal shortening and uplift of the Sierra Nevada of Santa Marta without significant isostatic compensation.

TCFAGA at the Guiana Craton are close to zero suggesting nearly complete isostatic

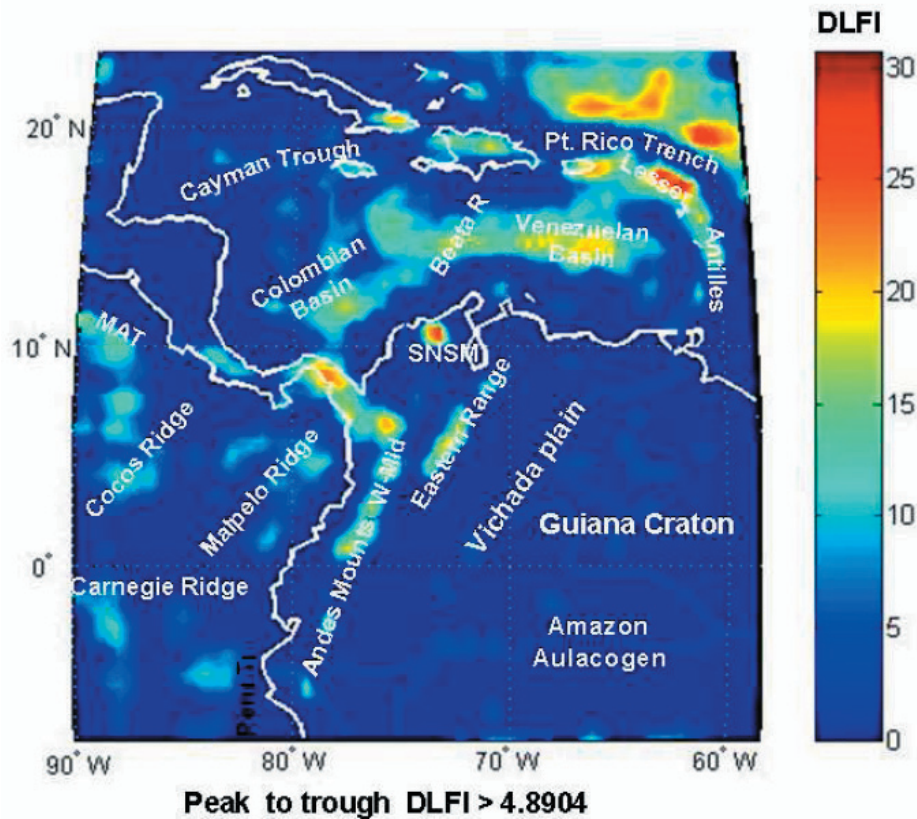


Figure. 10. Differenced local favorability indices (DLFI) between TCFAGA and FCTGE at 20 km elevation for the study region showing the TCFAGA-peak to FCTGE-trough associations for $DLFI > 4.8904$. SNSM= Sierra Nevada of Santa Martha, W-Mid =Western-Central ranges. This map was produced using the Albers equal-area conic projection.

compensation. Local TCFAGA highs and lows may reflect the occurrence of lateral mass variations related to intrusive bodies without topographic expression ($TGE = 0$). Here, the TCFAGA that are greater than the TGE give an example of overcompensated terrain. The negative TCFAGA along the Eastern Andes Mountains are associated with continent - continent convergence between the North Andes Microplate and the South American Plate with regional thrust faults dipping to the west and intensive compressional and transpressional deformation (Cediel *et al.*, 2003). Therefore, the negative TCFAGA along the eastern cordilleran area appear to reflect the thickening of the continental crust with thick sedimentary sequences that are known to contain oil and gas deposits (Stein & Sella, 2002).

4.5. TERRAIN-DECORRELATED FREE-AIR GRAVITY ANOMALIES

The TDFAGA in Figure 5 are very poorly correlated with TGE ($CC = -0.0575$) and mostly show gridded patterns due likely to observational and data processing noise. Thus, we do not consider the geological implications further for the TDFAGA.

4.6. TCFAGA AND FCTGE ANOMALY CORRELATIONS

Tectonic analysis of enhanced correlations between the TCFAGA and FCTGE are visualized better using summed local favorability indices with ($SFLI \geq 8.7226$) in Figure 8. High amplitude peak-to-peak zones along the Andes Mountains overlay mapped mineralized batholithic intrusions (INGEOMINAS, 1987). According to Kerr *et al.* (1997), subduction related batholiths

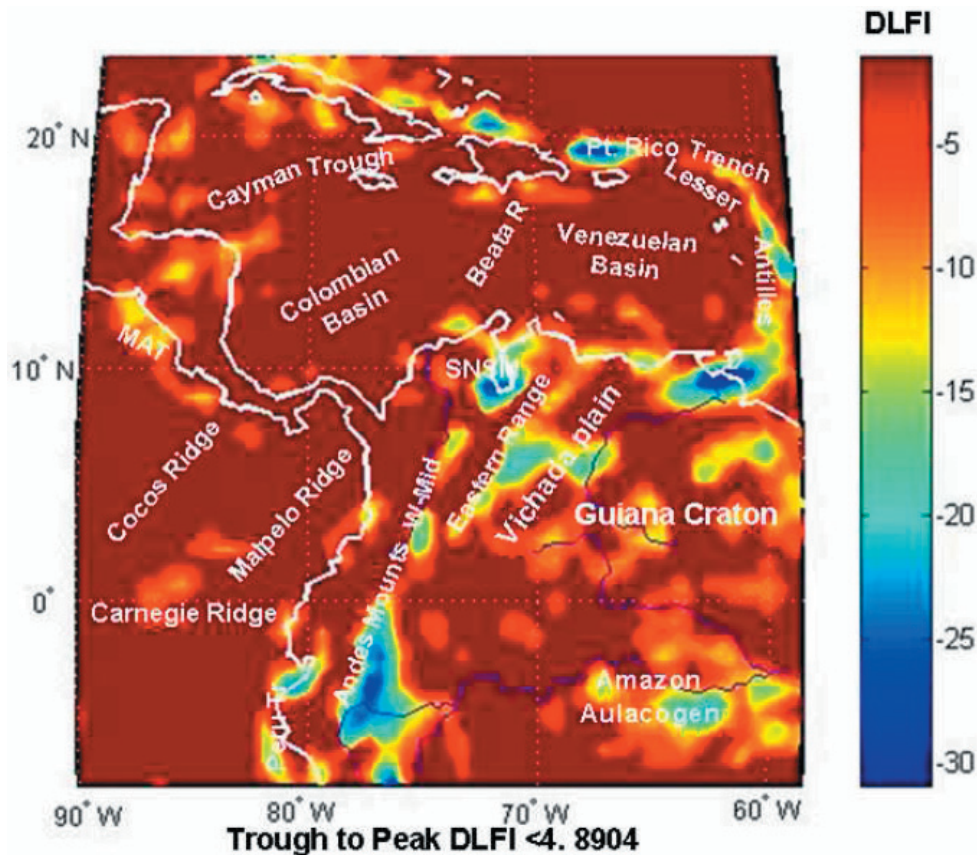


Figure 11. Differenced local favorability indices (DLFI) for TCFAGA and FCTGE at 20 km elevation for the study region showing the TCFAGA-trough to FCTGE-peak associations for $DLFI \leq -4.8904$. SNSM= Sierra Nevada of Santa Martha, W-Mid = Western-Central ranges. This map was produced using the Albers equal-area conic projection.

and extrusive rocks found around the margin of the Caribbean - Colombian cretaceous igneous provinces are of two distinct events: one suite represents the pre-plateau, collision-related volcanism, whereas the other suite, which is slightly younger than the plateau, may be associated with subduction. Therefore, peak-to-peak zones along the western Cordillera may be associated with subduction, whereas peak-to-peak zones along the eastern Cordillera are associated with the pre-plateau collision suite of igneous rocks.

Intermediate amplitude peak-to-peak correlations at the Guiana Craton also indicate isolated topographic highs on relatively denser intrusive rocks of the cratonic basement. These inferred intrusions may be the source rocks of known gold and diamond placer deposits of the Guainia and Orinoco rivers (Romero *et al.*, 1996).

The $SLFI \leq -8.7226$ in Figure 9 shows trough-to-trough correlations between TCFAGA and FCTGE, respectively. They clearly mark the Puerto Rico, Colombian and Peruvian Trenches, while the Middle American Trench and the Pacific Colombian Trenches are relatively poorly defined. The oceanic trenches are the most isostatically disturbed features in the area and also the most seismically active features. Of special interest are the intermediate trough-to-trough correlations of TCFAGA and FCTGE in the Colombian and Venezuela Basins. These areas are undergoing intensive exploration for oil and gas and have productive fields associated with delta deposits of the Magdalena River, the major supplier of sediments to the Caribbean Sea. Therefore, the SLFI anomaly correlations may mark strong prospective areas for locating sedimentary basins in the Caribbean plate.

The differenced local favorability indices with $DLFI \geq 4.8904$ show TCFAGA-peak to FCTGE-trough correlations in Figure 3.10. They mark topographic depressions that are overcompensated by local denser bodies along the Lesser Antilles, Colombian basin, western and central ranges, Sierra Nevada of Santa Marta and at the North American Plate. The TCFAGA-trough to FCTGE-peak correlations with $DLFI \leq 4.8904$ in Figure 3.11, on the other hand, show the distribution of low density zones along the eastern Andean Mountains, the upper Amazon River and lower Orinoco river. The negative DLFI zones mark mapped sedimentary basins including the upper, middle and lower Magdalena valley (UMV, MMV and LMV, respectively), and the Orito, Llanos, Maracaibo, Guajira and Orinoco basins with known productive oil and gas fields. Thus, the negative DLFI zone outlined at the upper Amazon river aulacogen may also infer a prospective sedimentary basin for oil and gas exploration.

5. CONCLUSIONS

The central parts of the Nazca, Cocos and Caribbean Plates are mostly in isostatic equilibrium with TCFAGA close to zero. This condition changes at the plate boundary zones and volcanic ridges. Positive TCFAGA are associated with the Malpelo, Cocos, Carnegie and Beata Ridges. TCFAGA may also be associated with dynamic topography by upwelling mantle. Thickening the oceanic crust by crustal roots into the mantle partially compensates for the TGE. In the case of the Malpelo Ridge, this volcanic range is partially compensated with a crustal root, in agreement with the seamount model proposed by Watts (2001) for isostatic compensation of seamounts and oceanic islands. Depth to the MOHO estimated from gravity data is supported by seismic data (Trummer, 2002). The Andes Mountains are isostatically disturbed. The Airy-type isostatic model is consistent with the thickening of the crust at the Andes Mountains, but lateral density variations between the oceanic and continental crusts must be involved to model TCFAGA. The Pratt-type isostatic model is not appropriate to model TCFAGA of the Andean Mountains because it can not account for the thick continental roots shown in the seismic data

(Trummer, 2002).

Locally positive TCFAGA anomalies in the Guiana Craton are associated with relatively denser intrusive bodies affecting the host cratonic rocks. These intrusive bodies do not have a significant surface expression and may be related to mass variations in the crust and upper mantle.

Compressional tectonics has played an important role in the mountain building of the North Andes Micro-plate as a consequence of the relative movements among Nazca, South America and Caribbean Plates and Panama and North Andes Micro-plates. The shortening associated with plate motion, based on GPS data only accounts for less than 50% of the mountain building (Lamb, 2004). Magmatic under-plating and crustal doubling due to over-thrusting may also contribute to the formation of the Andes Mountains and the Sierra Nevada of Santa Marta, as inferred by the positive TCFAGA.

Considering that isostatic equilibrium is the ideal state that any uncompensated mass tends to reach through time, implies that any uncompensated mass of the North Andes Mountains is under pressure to adjust vertically and horizontally to reach equilibrium. Therefore, a direct correlation is expected between disturbed and seismically active terrains, whereas minimal seismic activity is expected for isostatically compensated terrains (Artyushkov, 1973).

SLFI and DLFI enhance TCFAGA and FCTGE anomaly correlation, providing new criteria to locate areas for prospecting mineral and fossil fuel deposits.

The results presented here must be used with care. It has been assumed a simplification of the gravity effects at 20 km altitude, where a compensating mass at 35 km depth has only about 40% of the amplitude of the gravity signal of the surface mass that it compensates; therefore, positive and negative FAGA do not mean, on their own, a lack of compensation. For example, a maximum FAGA of about 184 mGal is greater than the roughly 110 mGal expected for fully compensated terrain, the difference reflects the

true lack of compensation.

ACKNOWLEDGMENTS

We thank Mohammad Asgharzadeh and Laramie Potts, from the Geological Sciences Department of the Ohio State University, for their assistance in the inverse gravity modeling. Elements of this research were supported from FULBRIGHT-LASPAU, Universidad Nacional de Colombia, COLFUTURO and Sociedad Minera Kedahda S.A.

REFERENCES

- Artyushkov, E. V. (1973). Stresses in the lithosphere caused by crustal thickness inhomogeneities. *Journal of Geophysical Research*. **78**. 7675-7708.
- Bird, P. (2003). An Updated digital model of plate boundaries, *Geochemistry, Geophysics Geosystems* **G3**. **4** (3).1-52.
- Cediel, F., Shaw, R. P., and Caceres, C. (2003). Tectonic assembly of the Northern Andes Block. The Circum-Gulf of Mexico and Caribbean Hydrocarbon habitats, basin formation and plate tectonics. *AAPG Memoir*. **79**. 815-848.
- Davis, J. C. (1986). *Statistics and data analysis in geology*: John Wiley & Sons Inc. New York, 646 pp.
- Dewey, J. F. and Pindell, J. L. (1985). Neogene block tectonics of eastern Turkey and Northern South America: Continental applications of the finite difference method. *Tectonics*. **4**. 71-83.
- von Frese, R. R. B. and Tan, L. (1999). Antarctic crustal modeling from spectral correlation of free-air gravity anomalies with the terrain. *Journal of Geophysical research*. **104** (11). 275-296.
- von Frese, R. R. B., Jones, M., Kim, J. W. and Kim, J. H. (1997). Analysis of anomaly correlations. *Geophysics*. **62** (1).342-351.
- von Frese, R. R. B., Alsdorf, D. E., Kim, J. H., Stepp, T. M., O'Connell, D. R. H., Hayden, K. J. and Li, W. S. (1992). Regional geophysical imaging of the Antarctic lithosphere, in *Recent Progress in Antarctic Earth Science*, edited by Yoshida, Y., Kaminuma, K., and Shiraishi, K. pp. 465-474, TERRAPUB, Tokio, Japan.
- von Frese, R. R. B. (1980). Lithospheric interpretation of satellite elevation gravity and magnetic anomaly data, PhD dissertation, Department of Geosciences, Purdue University, W. Lafayette, IN. USA. 1-164.
- INGEOMINAS (1987). *Recursos Minerales de Colombia*. Tomos I, II, Pub.Geol.Rsp.1, Bogota, 1119 pp.
- Kellogg J. N., Vega, V. Stalling, T. C., and Aiken, L. V. (1995). Tectonic development of Panama, Costa Rica and the Columbian Andes: Constraints from Global Position System geodetic studies and gravity, in *Geol. and Tect Devel of the Caribbean Plate boundary in Southern Central America*. *Geol. Soc. Am. Spec. Pap.* **295**. 75-86.
- Kellogg, J. N., Ogujiofor I. J. and Kansakar, D. R. (1985). Cenozoic tectonics of the Panama and North Andes blocks, *Mem. Congr. Latinoam. Geol.* **6**. 40-59.
- Kerr, A. C., Tarney, J., Marriner, G. F., Nivia, A., and Saunders, A. D. (1997). The Caribbean - Colombian Cretaceous Igneous Province: The Internal anatomy of an Ocean Plateau. *AGU Geophysical Monograph*. **100**. 123-144.
- Kim, J. W., von Frese, R. R. B., and Rae, K. H. (2000). Crustal modeling from spectrally correlated free-air and terrain gravity data A case study of Ohio. *Geophysics*. **65** (4). 1057-1069.
- Lamb, S. (2004). *Devil in the Mountain, A Search for the origin of the Andes*. Princeton University Press, New Jersey, 335 pp.
- Leftwich, T. E., von Frese, R. R. B., Potts, L. V., Kim, H. R., Roman, D. R., Taylor, P. T., and Barton, M. (2005). Crustal modeling of the North Atlantic from spectrally correlated free-air and terrain gravity. *J. Geodynamics*. **40**. 23-50.

- Lemoine, F. G., Chinn, D. S., Cox, S. M., Factor, J. K., Kenyon, S. C., Klosko, S. M., Luthcke, S. B., Olson, T. R., Pavlis, E. C., Pavlis, N. K., Rapp, R. H., Smith, W. H. F., and Sandwell, D. T. (1994). Bathymetric prediction from dense satellite altimetry and sparse shipboard bathymetry. *J. Geoph. Res.* **99**. 21803-21824.
- Liu M., Yang Y., Stein S., and Klosko, E. (2002). Crustal shortening and Extension in the Central Andes: Insights for a Viscoelastic model. *AGU Geod.* **30**. 325-339.
- MATHWORKS, inc. (2005). MATLAB version 7.0.4 352 (R14). <http://www.mathworks.com/>.
- Merriam, D. F. and Sneath, P. H. A. (1966). Quantitative comparison of contour maps. *J. Geophysical Research.* **7**. 1105-1115.
- Roman, D. R. (1999). An integrated Geophysical Investigation of Greenlands Tectonic History. PhD Dissertation. The Ohio State University, 1-270.
- Romero, F. H., Schultz, R. A., and Chavez, T. (1996). Ocurrencias diamantíferas de la quebrada Alba Rosa, caño Guapito, Guainia, Colombia. *Geol. Col.* **20**.
- Smith, W. H. F. and Sandwell, D. T. (1994), Bathymetric prediction from dense satellite altimetry and sparse shipboard bathymetry. *Journal of Geophysical research.* **99**. 21803-21824.
- Stein, S. and Freymueller, J. T. (2002). Plate Boundary Zones, editors. *AGU Geodynamic Series.* **30**. 425 pp.
- Stein, S. and Sella, G. F. (2002), Plate boundary zones: Concepts and approaches. *AGU Geodynamics series.* **30**. 1-26.
- Tan, L. and von Frese, R. R. B. (1997). Satellite geopotential models of East Asian Lithosphere (Abstract), Trans. AGU. Spring meeting supplements. **78**. 114-121.
- Trummer, I. (2002). S-Wave processing and interpretation of wide-angle seismic refraction data, Malpelo ridge, eastern Panama basin, PhD dissertation, der Mathematisch-Naturwissenschaftlichen Fakultät, der Christian Albrechts- Universität, Zu Kiel.
- Watts, A. B. (2001). Isostasy and flexure of the lithosphere. First edition, Cambridge University Press, New York, 458 pp.